

## **INFLUENCE OF DATABASE ACCURACY ON TWO DIMENSIONAL RAY TRACING BASED PREDICTIONS IN URBAN MICROCELLS**

Karim Rizk, *Student Member IEEE*, Jean-Frédéric Wagen, *Member IEEE* and Fred Gardiol, *Fellow IEEE*

**Abstract—Ray tracing based predictions in urban microcellular environments require databases for building layouts, electrical characteristics of buildings and base station (locations, antennas, power, etc.). The aim of this paper is to provide help in selecting the appropriate level of accuracy required in these databases in order to achieve the best tradeoff between database costs and prediction accuracy. The effects of inaccuracies in these databases are presented and analyzed by comparing predictions and measurements. The results presented here show to what extent errors, which are due to automatic vectorization of scanned maps, could lead to erroneous predictions. Furthermore, an analysis of the influence of random errors in a building vector database was performed to quantify the prediction error as a function of the accuracy in the building vector databases. Ray tracing prediction models implementing a reflection and diffraction phenomena were found to be sensitive to the choice of the reflection coefficient attributed to building walls. This dependence can be used to fit the measurements as the complexity of real building walls does not allow to easily derive their electrical parameters from which a reflection coefficient could be computed. It was also found that, in general and in agreement with measurements, ray tracing based prediction models are not sensitive to small variations on base station location. Finally, the sensitivity study also lead to gained insight of the propagation phenomena involved in urban microcell environments.**

### I. INTRODUCTION

The performance of a mobile radio communication system depends on the radio propagation environment. The drive to increase the capacity of cellular communication systems has led to, among other solutions, the introduction of the microcell concept. In order to confine the radio coverage within a small area, for example, less than about 300m in radius, in a typical microcell, the height of the base station antenna is lower than the average buildings height. In microcell environments, propagation models used for conventional larger cells may lead to poor accuracy since the predictions are based on computations over radials from the base station [1] and

thus do not take into account the radio energy which propagates around the buildings. Efforts made to derive more accurate models based on a ray tracing technique appear to be promising [2-6]. These models require databases for the building layout, the electrical characteristics of the buildings, and for the base station (locations, antennas, power, etc.). This paper addresses the problem of inaccuracies that might exist in some databases. As no database is error free, it is of great interest to quantify the prediction errors as a functions of database inaccuracies.

A preliminary study of the influence of inaccuracies in a building database on the predictions can be found in [7] and [8]. Unlike this paper, the results in [7] do not show the influence of the inaccuracies in the building database on the performance of the ray tracing model when compared to measurements. Similarly, [8] presents a preliminary investigation into the effects of inaccuracies in building databases and also analyzes the effects of the location of the base station.

The ray-tracing based model and a brief description of the measurements are described in the next section. The effects of inaccuracies in the vectored building layout are analyzed in Section III. The dependence of the predictions on the reflection coefficient is presented in Section IV. Section V shows the effects of inaccuracies related to the base station location. Other effects due to, for example, errors in the antenna pattern or in the antenna orientation are not considered here.

## II. MODEL DESCRIPTION AND MEASUREMENTS

The propagation prediction model used for this investigation is based on image theory and ray tracing. The inputs of the model are: **1) the two-dimensional geometry described by means of vectors specifying the location and position of building walls, 2) the estimated electrical characteristics of the building walls** (through either their permittivity and conductivity or a constant scalar reflection coefficient), **3) the base station antenna location**, orientation, tilt and height, **4) the antenna pattern**, and **5) the frequency**. In this paper, the influence of inaccuracies and variations to the building wall vector data, the electrical characteristics of the building walls, and the base station locations are discussed.

The computations presented here account for specular reflections from building walls and single diffractions from building corners. Ground reflections and rays over rooftops are neglected. The software computes all combinations rays reflected and/or once-diffracted up to some predetermined order. The ray tracing computation

is performed according to a careful implementation of image theory where vectors, or parts of vectors not in line-of-sight of a given source do not produce image-sources. Thus, the computation time is kept reasonable since the exponential complexity of a brute force image method is drastically reduced at the expense of only minor additional processing. The algorithm used to determine image-sources is described in [9]. In order to take into account diffraction effects, virtual sources are placed on every illuminated building corner. The virtual sources of diffractions are then used to generate higher order image-sources. All possible combinations of reflected and once-diffracted rays that reach a mobile are determined after all image and virtual sources have been created. Then, all rays can be traced and their associated wave field computed. Note that starting from the original source at the base station antenna location, the image sources and the virtual sources depend only on the building layout, i. e., on the vectors describing the building walls. Therefore, the generation of the image and virtual sources does not depend on the location of the mobile (i.e., the observation point). Furthermore, our ray tracing algorithm [9] can handle an arbitrary layout of buildings without any restriction on building shape as long as it can be described by vectors.

The reflected wave fields are computed using either the well known formula for the Fresnel reflection coefficient, or a scalar constant reflection coefficient. Since this investigation is relevant to mobile communications where the base station antennas usually radiate a vertically polarized wave, the electric field is assumed to be parallel to the building walls (vertical polarization). The diffracted wave fields can be computed using a diffraction coefficient valid for either **a**) perfectly absorbing wedges [10], **b**) perfectly conducting wedges [11] or **c**) wedges with impedance faces [12]. In [9], it was found that these three diffraction coefficients result in comparable coverage predictions when used in a ray tracing model applied to a real urban environment. Therefore, in this paper the diffraction coefficient that is valid for perfectly absorbing wedges and that has the simplest expression is considered.

Building walls are made of several materials (concrete, brick, various type of glass, etc.). However, different buildings in a given area are generally made of similar materials, and therefore the results presented here assume that all building walls have the same value for their electrical characteristics. The values of these electrical characteristics are determined by preliminary comparisons with measurements. Unless otherwise noted, the electric relative permittivity and the conductivity of building walls have been chosen to equal to  $\epsilon_r = 5$  and  $\sigma = 10^{-4}$  [S/m], respectively.

In the model the following phenomena are taken into account: the direct (Line-Of-Sight or LOS) ray when it exists; up to 9 reflections, or all possible combinations of up to 8 reflections and a single diffraction per path. The maximum number of reflections (reflection order) is closely related to electrical parameters of building walls, and should be selected in such a way that taking a larger reflection order will not significantly change the computation results. When using the electrical parameters mentioned above, this condition was found to be fulfilled with an order equal to nine. The path loss is computed by adding up the power of every ray. In [5], vector summing was preferred as discrepancies were found between vector summing and power summing for receivers far from the transmitter. In this investigation however, the receivers are within a relatively small radius from the transmitter (less than 300 m). The power summing is thus used to clarify the figure by smoothing the results without losing necessary information.

In order to make a comparison with measurements, the path loss is computed every 1 or 2 m along a line on the street where measurements were taken.

The measurements considered here were undertaken in Bern (Switzerland). Bern is a small European city characterized by an irregular layout of buildings. The measurements though, were performed in an area with almost perpendicular street crossings in an attempt to simplify the investigation of radio propagation mechanisms. The map of the area considered in our predictions is shown in Fig. 1. The circles indicate the considered positions of the sources (transmitters). The segments with arrows indicate the measurement paths. The area considered is characterized by a somewhat irregular layout, 3-4 stories concrete buildings, narrow streets (~10-15 m), some trees and little traffic as expected in a residential area. The street denoted "Rodtmatt St." in Fig. 1 however, is a two lane street with some traffic.

Measurements have been carried out at 1890 MHz with a commercial omni-directional stacked dipole array placed at approximately 6m above ground and with a car mounted quarter-wave monopole (height: 1.5 m). Measurement samples were recorded every 1.75 m. For the transmitter  $Tx3$  (Fig. 1) a time trigger was used rather than a distance trigger to record the measurements. Therefore, a possible shift between measurements and predictions could appear although care was taken to drive at a constant speed. The measurements are described with more detail in [9].

### III. BUILDING LAYOUT DATABASE

The prediction model described above requires the two-dimensional building layout of the considered urban area as given by means of vectors describing the building walls. Predictions based on the building layouts for the same area but derived from three different types of maps are presented in this section. The three types of maps are: a cadastre map, a city map and a 1:25000 scale map. First, in parts A, B, and C, predictions and measurements for a mobile receiver traveling along Rodtmatt street will be used to illustrate the effects of map inaccuracies. Finally in part D, artificial random errors are introduced in the most accurate map, and the resulting prediction errors are discussed.

#### *A. Vectors from the cadastre map*

The cadastre maps are usually available for any city, although they may not be easily obtained. They are mainly used as a legal reference to determine the boundary of properties and therefore, are very accurate. In Switzerland this type of map is usually available only on paper. Therefore, the vectors shown in Fig. 1 were obtained by hand vectorization using a digitizing tablet. The resulting accuracy is about half a meter on the location of the building corners.

In Fig. 3, predictions using the cadastre map are compared to measurements on Rodtmatt St. for the transmitter location labeled  $Tx3$  in Fig. 1. A reasonable agreement between measurements and predictions is observed. The mean error and standard deviation between predictions using the cadastre map and measurements are 4.7 dB and 6.6 dB respectively.

#### *B. Vectors from the city map*

City maps are available almost anywhere on paper as they are sold for general purpose including private businesses and tourism. The vectors used here were also obtained by hand vectorization from a paper city map. Comparisons on Rodtmatt St. between measurements and predictions using the city map are presented in Fig. 3. It can be seen that the predictions using the city map vectors overestimate the measured received power along most of the street. The larger received power in the predictions is due to wrong street widths. Indeed, the width of streets on a city map may be drawn larger for clarity, i.e., to represent the importance of the street and to allow the street name to be written. Also, the details of building blocks are omitted most of the time. The effects of these types of errors are even better illustrated in the next section.

The mean error and standard deviation between predictions using the city map and measurements (predictions using the cadastre map) are 10.3 dB (5.6) and 9.2 (6.81) dB respectively.

### *C. Vectors from the 1:25000 map*

The last type of vectors considered are those extracted from 1:25000 scanned maps. In fact, these maps are currently the only sort of maps available in an electronic format for almost all of Switzerland. Special recognition algorithms were applied on the scanned maps to recognize the buildings from other features on the map [13]. The vectorization presented here used the following three steps: 1) automatic recognition of buildings (to eliminate text, special characters, railways, etc.), 2) manual correction of errors from automatic recognition, and 3) automatic vectorization.

Fig. 4 shows the resulting vector map based on the 1:25000 scaled map. The comparison on Rodtmatt St. between measurements and predictions using the 1:25000 map and the cadastre map is presented in Fig. 5. It can be seen that the predictions using the 1:25000 map underestimate the measured power along the whole street. The underestimation is mainly due to errors in the automatic vectorization. In fact, because of the representation of the scanned 1:25000 map, the sidewalk could not be separated from the buildings, thus leading to narrower streets (for example between Bldg. 1,2 and 3 in Fig. 4). Also, the peak in the measurement at  $d \approx 75$  m (Fig. 5) is missed in the predictions since Bldg. 3 and Bldg. 4 are joined together. This is due to an error in the automatic building recognition. The missing peak in the predictions based on the 1:25000 maps shows the extent to which much details of building blocks are at times needed for the ray tracing model.

The mean error and standard deviation between predictions using the 1:25000 scanned map and measurements (predictions using the cadastre map) are -17.6 dB (-22.3) and 6.6 (6.6) dB respectively.

Because of the errors in the automatic vectorization, it was necessary to add a fourth to the three vectorization steps mentioned above step involving the manual correction of the buildings. The predictions using the resulting corrected vectors were comparable to those obtained using the cadastre maps. They are not shown here.

### *D. Maps with random errors*

The predictions presented above based on three different types of maps showed the sensitivity of the predictions to the inaccuracies that might exist in different maps. To quantify the largest acceptable error we analyze, in the following the influence of random errors artificially introduced in the cadastre map. The random errors are

generated using generators of normal and uniform distributions [14] as shown in Fig. 6. As in [7] two types of errors are considered:

- a) Errors in the building size while keeping the orientation of building walls (Fig 6.a), i.e., the building walls are displaced parallel to their original locations, the magnitude of the displacement is chosen randomly for each wall from a normal distribution with zero mean and standard deviation  $\sigma$ .
- b) Errors in the vertex position or corner location of a building (Fig. 6.b), i.e., the building corners are displaced randomly and uniformly around their original location. The radial displacement is taken from a normal distribution with zero mean and standard deviation  $\sigma$ .

For each type location error, the following four standard deviations are considered:  $\sigma = 0.5$  m,  $\sigma = 1$  m,  $\sigma = 1.5$  m, and  $\sigma = 2$  m. By definition of the normal distribution, 95% of the vertices or of the building wall displacements are within an interval of  $[-2\sigma, +2\sigma]$  from their original position. For each of the 8 cases determined by a type of error (denoted  $i=a, b$ ) and a value of  $\sigma$ , 25 maps or realizations were generated with different seed, starting from the cadastre map (Fig. 1) as the original map. Thus, 200 erroneous maps have been generated. Considering the transmitter location labeled  $Tx21$  (Fig. 1), predictions based on the erroneous maps were compared to: 1) the measurements and 2) the predictions using the original cadastre map. The comparisons were performed on 858 test points uniformly distributed on all the observation routes shown in Fig. 1, except Rodtmatt St. Note that Rodtmatt St. was excluded because there is a tunnel in the building south of the transmitter location  $Tx21$ . This tunnel between Breitfeld St. and Rodtmatt St. is not present in our database but was noticed during an on site investigation. This tunnel provides a propagation path leading to a large prediction error on Rodtmatt St.

Let  $ERR_m$  be the error resulting from the difference between the predicted received power using the erroneous maps and the measured received power:

$$ERR_m = P_p(\text{test point } j, \text{ error type } i, \sigma) - P_m(\text{test point } j)$$

$ERR_m$  determines how the accuracy of the building database influences the accuracy of the model.

Similarly, let  $ERR_p$  be the error resulting from the comparisons between the predictions using the erroneous maps and the predictions using the original cadastre map.

$$ERR_p = P_p(\text{test point } j, \text{ error type } i, \sigma) - P_p(\text{test point } j, \text{ NO ERROR})$$

$ERR_p$  is an indication of the model sensitivity to the building database.

For each realization, error type and value of  $\sigma$ , the  $ERR_m$  or  $ERR_p$  values on the 858 test points along the measurement routes are treated as random variables characterized by their means  $E[ERR_m] = A_{ERRm}$  and  $E[ERR_p] = A_{ERRp}$  and their standard deviations  $\sigma_{ERRm}$  and  $\sigma_{ERRp}$ . Averaging over the 25 realizations provides the average values  $E[A_{ERRm}]$ ,  $E[A_{ERRp}]$ ,  $E[\sigma_{ERRm}]$  and  $E[\sigma_{ERRp}]$  for each error type and value of  $\sigma$ . Furthermore, the following standard deviations are computed over the 25 values:  $\sigma(A_{ERRm})$ ,  $\sigma(A_{ERRp})$ ,  $\sigma(\sigma_{ERRm})$ , and  $\sigma(\sigma_{ERRp})$ .

The four averaged values are plotted in Fig. 7 as a function of  $\sigma$ . Also plotted in Fig. 7 are the upper and lower values ( $\text{mean} \pm 2 \cdot \text{STDEV}(\cdot)$ ) representing the 95% confidence interval, which was computed under the assumption that  $E[A_{ERRm}]$ ,  $E[A_{ERRp}]$ ,  $E[\sigma_{ERRm}]$  and  $E[\sigma_{ERRp}]$  are normally distributed. The four computed averages ( $E[A_{ERRm}]$ ,  $E[A_{ERRp}]$ ,  $E[\sigma_{ERRm}]$  and  $E[\sigma_{ERRp}]$ ) are indeed normally distributed according to the central limit theorem [15] since:

1) for each realization, the values  $A_{ERRm}$ ,  $A_{ERRp}$ ,  $\sigma_{ERRm}$  and  $\sigma_{ERRp}$  are independent random variables as they are the result of independent random variations on the original map, 2) the 25 realizations, and thus the 25 values  $A_{ERRm}$ ,  $A_{ERRp}$ ,  $\sigma_{ERRm}$  and  $\sigma_{ERRp}$  are identically distributed, 3) the values  $E[A_{ERRm}]$ ,  $E[A_{ERRp}]$ ,  $E[\sigma_{ERRm}]$  and  $E[\sigma_{ERRp}]$  are sample averages, i.e., sums of independent identically distributed random variables. Therefore,  $E[A_{ERRm}]$  for example, is itself a random variable with normal distribution  $N(E[A_{ERRm}], \sigma(A_{ERRm}))$ , that has a mean equal to  $E[A_{ERRm}]$  and a standard deviation equal to  $\sigma(A_{ERRm})$  [15]. The number of realizations considered here (25) is sufficiently large to accurately characterize the statistical distribution.

Fig. 7 can be used to evaluate: 1) by how much a certain level of error in the building databases will deteriorate the accuracy of the predictions when compared to measurements or 2) how different the predictions with the erroneous maps are from the predictions using an error free map.

When analyzing the results presented in Fig. 7, it is important to mention that, with respect to the measurements, when the reference map is used, the mean error and the standard deviation of the prediction results, are 0.2 dB and 7.36 dB, respectively.

The behavior of the standard deviation  $E[\sigma_{ERRm}]$  and  $E[\sigma_{ERRp}]$  in Fig. 7.b and d shows that a smaller prediction error occurs when the errors in the building database do not affect the orientation of the building walls. In [7], it was also found that predictions are more sensitive to errors that affect the orientation of building walls than those which affects building size. Therefore, when producing the building layout database needed for the ray tracing technique, a special care has be taken to keep the orientation of the building walls as accurate as possible. It is also possible to correct the data base vectors by taking advantage of the fact that building walls forming a street are generally parallel.

From Fig. 7.a and c, it can be observed that the mean errors for the case of vertex errors are independent of the standard deviation  $\sigma$  of the location error. In the case of errors in building size, the mean prediction errors increase in absolute value as the standard deviation  $\sigma$  of the location error increases. This leads to the conclusion that the mean prediction error is more sensitive to errors in the street width than to errors in the parallelism of building walls along a street. In Fig. 7.a and c  $E[ERR_m]$  and  $E[ERR_p]$  have similar values. This is because, for any level of error, the difference between  $E[ERR_m]$  and  $E[ERR_p]$  is equal to the mean error between predictions using the reference map and measurements, i.e. -0.2 dB.

Based on the normal distribution of  $E[A_{ERRm}]$ ,  $E[A_{ERRp}]$ ,  $E[\sigma_{ERRm}]$  and  $E[\sigma_{ERRp}]$  discussed above, Table 1 shows the probability that a certain degree of error in the building databases: 1) will increase the standard deviation between predictions and measurements by less than 0.5 or 1 dB or 2) will generate a standard deviation lower than 3 dB and 5 dB, between the predictions using the erroneous maps and the predictions using an error free map. The influence of the accuracy of the building database on the accuracy of the model, i.e.  $E[\sigma_{ERRm}]$ , exhibits significantly different behavior from the model sensitivity to the building database, i.e.,  $E[\sigma_{ERRp}]$ . It is for this reason that in Table 1 two different sets of thresholds (0.5 and 1 dB for the comparisons with measurements, and 3 and 5 dB for the comparisons with the reference prediction) were chosen.

Table 1 shows:

- 1- the probability of larger prediction errors is greater in the case of errors in building vertices as compared to the case of errors in the building sizes. Thus errors in building vertices lead to more inaccurate prediction results than errors in the building sizes. This is to be expected since the errors in building vertices may completely destroy the waveguiding effect due to parallel building walls along a street.

- 2- there is a 90% probability that the errors in building database will not increase the standard deviation of the prediction error, by more than 1 dB with respect to the measurements: **1)** if 95% of the building walls are within  $\pm 2$  m from their “real” position ( error in the building wall is characterized by  $\sigma \leq 1$  m, see Fig. 6.a), or **2)** if 95% of the building vertices are within  $\pm 1$  m from their “real” position (error in the vertex position characterized by  $\sigma \leq 0.5$  m, see Fig. 6.b).
- 3- there is a 90% probability that the errors in building database will not lead to a standard deviation larger than 5 dB with respect to the reference prediction: 1) if the error in the building wall is characterized by  $\sigma \leq 1$  m or 2) if the error in the vertex position is characterized by  $\sigma \leq 0.5$  m.

**Table 1** Influence of the errors in the building database.  $\sigma$  is the standard deviation of the error in building database (Fig. 6)

(a) Probability of **increasing** the standard deviation of the prediction error by **less than 0.5dB**:with respect to measurements

$\sigma$ [m]	Error in bldg. Size	Error in vertex
$\sigma=0.5$ m	<b>80%</b>	<b>24%</b>
$\sigma=1.0$ m	<b>77%</b>	<b>34%</b>
$\sigma=1.5$ m	<b>68%</b>	<b>48%</b>
$\sigma=2.0$ m	<b>45%</b>	<b>70%</b>

(b) Probability of **increasing** the standard deviation of the prediction error by **less than 1 dB** with respect to measurements:

$\sigma$ [m]	Error in bldg. Size	Error in vertex
$\sigma=0.5$ m	<b>95%</b>	<b>95%</b>
$\sigma=1.0$ m	<b>93%</b>	<b>86%</b>
$\sigma=1.5$ m	<b>88%</b>	<b>76%</b>
$\sigma=2.0$ m	<b>65%</b>	<b>49%</b>

(c) Probability of **having** a standard deviation of the error **smaller than 3 dB** with respect to the reference prediction:

$\sigma$ [m]	Error in bldg. size	Error in vertex
$\sigma=0.5$ m	<b>71%</b>	<b>7%</b>
$\sigma=1.0$ m	<b>92%</b>	<b>1%</b>
$\sigma=1.5$ m	<b>4%</b>	<b>1%</b>
$\sigma=2.0$ m	<b>2%</b>	<b>1%</b>

(d) Probability of **having** a standard deviation of the error **smaller than 5 dB** with respect to the reference prediction:

$\sigma$ [m]	Error in bldg. size	Error in vertex
$\sigma=0.5$ m	<b>99%</b>	<b>92%</b>
$\sigma=1.0$ m	<b>93%</b>	<b>32%</b>
$\sigma=1.5$ m	<b>55%</b>	<b>11%</b>
$\sigma=2.0$ m	<b>26%</b>	<b>3%</b>

Two realizations of erroneous maps due to errors in building size and in the building vertex position (using  $\sigma = 2$  m) are shown in Fig. 8.a and 8.b, respectively. It can be seen that the overall shape of the building layout is more altered when the errors affect the locations of building corners, i.e., the vertex positions.

For the two types of artificial errors introduced in the maps, and for several values of  $\sigma$ , the values of the field strength computed on our 858 test points were used to plot a probability density function of the prediction errors  $Err_p$ . Two typical probability density functions for  $\sigma = 1$  m are shown in Fig. 8 a and b, for the case of errors in building size and in the vertex position, respectively. For comparison, the probability density function for a log-normal distribution that has the same average and standard deviation as the 858 test points is also plotted. It is seen that  $Err_p$  is not normally distributed although  $E[A_{ERRp}]$  and  $E[\sigma_{ERRp}]$  were found to follow a normal distribution as shown above.

#### IV. REFLECTION COEFFICIENT

In this section we consider the sensitivity of the predictions when varying the reflection coefficient, which is attributed to the building walls. Predictions using different reflection coefficients are compared to: 1) the measurements and 2) a reference prediction. The reference prediction uses the reflection coefficient parameters which best fit the measurements (i.e.,  $\epsilon_r = 5, \sigma = 10^{-4}$ ).

The influence of several reflection coefficient values were already presented in the form of a table in [9]. Here, more values are considered and discussed. First, Fresnel reflection coefficients are considered assuming six different values of the wall permittivity:  $\epsilon_r = 2, 4, 5, 6, 8, 10$ . The wall conductivity is taken as a constant low value:  $s = 10^{-4}$  [S/m]. The second set of reflection coefficients are given by five different scalar coefficients  $R$  independent of the incidence angle:  $R=0.3, 0.446, 0.5, 0.562, 0.7$ . Scalar reflection coefficients were considered because they could lead to faster computations since they involve only a single real multiplication per reflection. The two values  $R=0.446$  and  $R= 0.562$  correspond to a 3 and 6 dB loss per reflection, respectively.

The mean error and standard deviation between predictions and measurements or the reference prediction when the permittivity varies, are shown in Fig. 10.a and b. The mean error and standard deviation between predictions and measurements, or the reference prediction when the  $R$  varies are shown in Fig. 10.c and 10.d. It is observed that the predictions are more sensitive to variations on the lower values of the permittivity. In fact, decreasing  $\epsilon_r$

from the ideal value of 5 to 2 has the following consequences: with respect to the measurements, it drastically increases the absolute value of the mean prediction error by 8 dB while only increasing the standard deviation by less than one decibel from 7.3 to 8.1 dB, i.e., predicted received power values are too small and thus, the predictions become pessimistic. This is not surprising as low permittivity indicates a weaker reflection and thus weaker guiding of energy along the streets. When increasing the wall permittivity  $\epsilon_r$  from 5 to 8, the mean prediction error increases by 4.5 dB while the standard deviation increases only by about half a decibel from 7.3 to 7.9 dB. The high sensitivity of the prediction mean error with respect to the reference prediction on variations of the lower values of the permittivity, directly follows from the high sensitivity of the Fresnel reflection coefficient on variations of the lower values of the permittivity [9]. It remains to be investigated why the standard deviation of error with measurements exhibits less sensitivity than the mean error to the variations of the permittivity.

Using a scalar reflection coefficient means that the reflection coefficient is independent of the incidence angle. It also means that the computation time can be slightly decreased. However, the scalar reflection chosen to give a mean error with the measurements close to zero, leads to a larger standard deviation of the prediction error: 9.3 dB instead of the 7.3 dB obtained with a Fresnel reflection coefficient (with  $\epsilon_r = 5, \sigma = 10^{-4}$ ). This hints at the importance of the incidence angle in the propagation phenomena. Note that other researchers used two different reflection losses depending on the angle of incidence [16]. The performance of this scheme with regards to the Fresnel reflection coefficient is beyond the scope of this paper.

The values of the field strength computed on our 858 test points were used to plot a probability density function of the prediction errors due to the varying reflection coefficient from the reference value ( $\epsilon_r = 5, \sigma = 10^{-4}$ ) to the different reflection coefficients listed above. Two typical probability density functions are plotted in Fig. 11 a and b, for the reflection coefficient given by  $\epsilon_r = 8, \sigma = 10^{-4}$  and for a 6 dB constant loss per reflection, respectively. For comparison, the probability density function for a log-normal distribution having the mean of 4.5 dB (-0.2 dB) and standard deviation of 2.3 dB (3.1 dB) is also plotted. The density functions in Fig. 11 show that the varying relative permittivity  $\epsilon_r$  from 5 to 8 leads to an error which does not follow a log-normal distribution. A uniform distribution would be a better approximation. However, considering a reflection coefficient independent of the angle of incidence leads to an error that is nearly log-normally distributed. A physical explanation of these distributions remains to be investigated.

V. BASE STATION LOCATION

In this section the prediction errors resulting from inaccuracies of the base station location are discussed. A preliminary study of this effect was performed in [8]. Here we complete our previous investigation by considering more than one measurement route. In [8], three predictions were computed using three base station locations separated by a few meters and located around the transmitter locations labeled  $Tx21$  in Fig. 1. The predictions on the Wiesen St., were found to be sensitive to the small variation of the base station location. In order to check if the measurements could be as sensitive to the transmitter location as the prediction results presented in [8] are, additional measurements were carried out using the following three base station locations:  $Tx21$ ,  $Tx22$ ,  $Tx23$ , the last two being less than 3 m from  $Tx21$  as shown in Fig. 1. These measurement are compared to predictions using the three base station locations on our test route, i.e. 858 test points uniformly distributed on all the observation routes shown in Fig. 1, except Rodtmatt St. Taking the location  $Tx22$  as a reference, the measurement (prediction) sensitivity to the base station location is shown in Table 3.a (3.b). The standard deviation between two sets of measurements or between two sets of predictions is used as a measure of sensitivity. It is pointed out that both measurements and predictions exhibit a small sensitivity to the variation of the base station location since the standard deviation never exceeds a value of about 4 dB in all the comparisons.

**Table 3** the standard deviation resulting from comparisons between two predictions and between two measurements considering two base stations located near each other in Fig. 1:  $Tx22$  and  $Tx23$ ,  $Tx22$  and  $Tx21$

(a) Measurement sensitivity		(b) Prediction sensitivity	
(Reference measurement: $Tx22$ )		(Reference prediction: $Tx22$ )	
<i>Transmitter locations</i>	<i>Std deviation [dB]</i>	<i>Transmitter locations</i>	<i>Std deviation [dB]</i>
$Tx22$ and $Tx23$	4	$Tx22$ and $Tx23$	4.3
$Tx22$ and $Tx21$	4	$Tx22$ and $Tx21$	3

Furthermore, although not shown in this paper, any set of two predictions computed using the transmitters  $Tx21$ ,  $Tx22$  or  $Tx23$  exhibits very close behavior on almost all the observation points. However, among the 848 observation points considered, the predictions for the observation points on Wiesen St. were found to exhibit the worst case, i.e., a high sensitivity to the transmitter location. Fig. 12 (Fig. 13) shows comparisons on Wiesen St. between two measurements (two predictions) considering the two base stations:  $Tx22$  and  $Tx23$ . As already

shown in [8] and in disagreement with the measurements, the effect of the base station location is predicted to be very important on Wiesen St. The discrepancy between the sensitivity of the prediction results and the relative insensitivity of the measurement results to the base station location could be due to a rather particular layout of buildings and transmitter location and/or to neglected effects such as trees which are not yet considered in the model.

## VI. CONCLUSIONS

The effects of some inaccuracies in the databases which are required for ray-tracing-based-predictions in urban microcellular environments have been presented. The databases considered included those for the building layout, electrical characteristics of the buildings and base station locations. Predicted results were presented and analyzed by comparison to measurements.

Three different maps were used to produce the building vectors used for the predictions, a cadastre map, a city map and a 1:25000 scaled map. The results improved with the accuracy of the geometry, giving the best results to the cadastre map which is the most precise one. Errors in building layouts which could occur when blindly applying automatic recognition algorithms on scanned maps could lead to erroneous prediction results. The details of each building block, especially openings, are also important for accurate predictions.

The influence in the predictions of two types of random errors or inaccuracies in building databases were analyzed. It was found that the predictions are more sensitive to errors in the building corner (vertex) position than to errors in the building size. The main difference between these two types of errors is that the orientation of building walls is affected in the case of errors in building corner position, whereas the orientation of building walls is kept constant in the case of errors in building size. In the example of Bern cited in this paper, it was found that to be 90% confident that the errors in building database will not increase the standard deviation by more than 1 dB with respect to the measurements, it is admissible for 95% of building walls to be within  $\pm 2$ m of their actual position. The same error in the standard deviation with the measurements can be obtained from an error in the building database in which 95% of building vertices are within  $\pm 1$  m from their actual position. Similar investigations in different environments are needed to determine how these error thresholds are dependent on the environment.

Various reflection coefficients were considered either in terms of the permittivity and conductivity (according to the Fresnel law), or in terms of a scalar coefficient which is independent of the incidence angle. The model was found to be sensitive to variations of the reflection coefficient especially for the lower value of the relative permittivity. The model sensitivity to the relative permittivity is similar to the sensitivity of the Fresnel reflection coefficient to the relative permittivity. Using a scalar reflection coefficient independent of the incidence angle has the likely advantage of decreasing computation time. However, it leads to less satisfactory predictions than those obtained with a Fresnel reflection coefficient.

Predictions and measurements were performed for three transmitter locations separated by a few meters. In general, and in agreement with measurements, the ray tracing model was found to be not too sensitive to variations of the transmitter location within a few meters. However, a high sensitivity was observed on one particular street where the model -but not the measurements- showed quite different results depending on the transmitter location. The discrepancy between the predictions and the measurements could be due to a rather particular layout of buildings and transmitter locations and/or to neglected effects such as trees which are not yet considered in the model.

The specular reflection computed according to the Fresnel law was confirmed to be an important phenomenon in the microcellular propagation. In fact, altering the specular reflections either by changing the building wall orientation or neglecting the angle of incidence in the reflection formulae increases the error between predictions and measurements.

REFERENCES

- [1] Loew, K., "Comparison of urban propagation models with CW-measurements", *Proc. Vehicular Technology Conf., Denver*, pp. 936-942, May 1992
- [2] Piazza, L., Bertoni, H. and Seongcheol K., "Comparison of measurements based and site specific ray based microcellular path loss predictions ", *Proceedings IEEE ICUPC*, Cambridge, Sept. . 1996.
- [3] Tan, S.Y., D. and H. S. Tan, "UTD propagation model in urban street scene for microcellular communications", *IEEE Trans. EMC*, Vol. 35, No. 4, pp. 423-428, Nov. 1993.
- [4] Bergljung, C. and L. G. Olsson, "Rigorous diffraction theory applied to street microcell propagation", *Proceedings GLOBECOM'91*, Phoenix, Arizona, pp. 1292-1296, Dec. 1991.
- [5] Erceg, V., Rustako, A. J. and Roman R. S. "Diffraction around corners and its effects on the Microcell coverage area in urban and suburban environments at 900 MHz, 2 GHz, and 6 GHz", *IEEE Trans. Trans. Vehic. Technol.*, Vol. 43, No. 3, pp. 762-766, August. 1994.
- [6] Schaubach, K. R., Davis, N. J., Rappaport, T. S., "A ray tracing method for predicting path loss and delay spread in microcellular environments", *Proc. Vehicular Technology Conf., Denver*, pp. 932-935, May 1992
- [7] Grace, D., Burr, A. G., Tozer, T. C., "The effects of building geometrical displacement error on urban microcellular ray based modeling Environments", *Proceedings IEEE PIMRC'94*, September 18-23, 1994, The Hague, Netherlands.
- [8] Rizk K., Wagen J. F., Khomri S. and Gardiol F., "Influence of Databases Accuracy on Ray-Tracing-Based-Prediction in Urban Microcells", *Proceedings IEEE 45th Vehicular Technology Conference*, pp. 252-256, Chicago, USA, July 1995.
- [9] Rizk K., Wagen J. F., and Gardiol F., "Two Dimensional Ray Tracing Modeling For Propagation Prediction In Microcellular Environments", *IEEE Trans, Veh. Technol.* vol. 46, May 1997, pp. 508-518
- [10] Felsen, L. B., and N. Marcuvitz, *Radiation and Scattering of Waves*, Prentice-Hall, Inc., Englewood Cliffs, New Jersey, 1973. Sec. 6.4.
- [11] Kouyoumjian, R. G., P. H. Pathak, "A uniform geometrical theory of diffraction for an edge in a perfectly conducting surface", *Proc. IEEE*, pp. 1448-1468, Nov. 1974.
- [12] Luebbers R. J. "Finite conductivity uniform GTD versus knife edge diffraction in prediction of propagation path loss", *IEEE Trans. AP*, Vol. 32, No. 1, pp. 70-76, Jan. 1984.
- [13] Nebiker, S., and A. Carosio, "Automatic extraction and structuring of objects from scanned topographical maps", *Proceedings SPRS Symposium on Primary Data Acquisition and Evaluation*, Vol. 30, Part 1, Como, Italy, 1994.
- [14] Press, W. H., Teukolsky, S. A., Vetterling W. T., Flannery, B. P., *Numerical recipes in C*, Cambridge University press, 1992. Sec. 7
- [15] James, G., *Modern Engineering Mathematics*, Addison Wesley, 1993. Sec. 10.3.
- [16] Seidel, S. Y., Schaubach K. R., Tran T., and Rappaport T. S., "Research in site-specific propagation modeling for PCS system design," *Proceedings IEEE 43th Vehicular Technology Conference*, p 261-263, Secaucus, NJ, USA 1993.

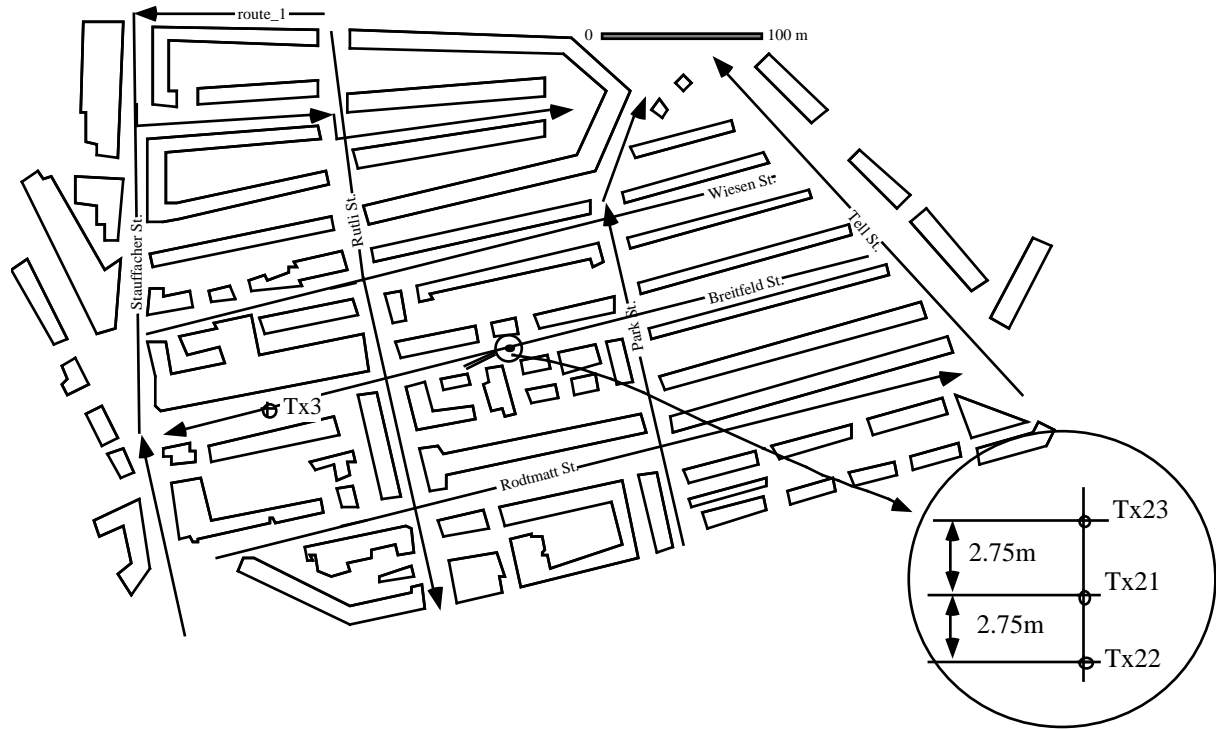


Fig. 1. Cadastre map. The circles indicate the transmitter locations. The arrowed lines represent the observation routes driven in the direction indicated by the arrow.

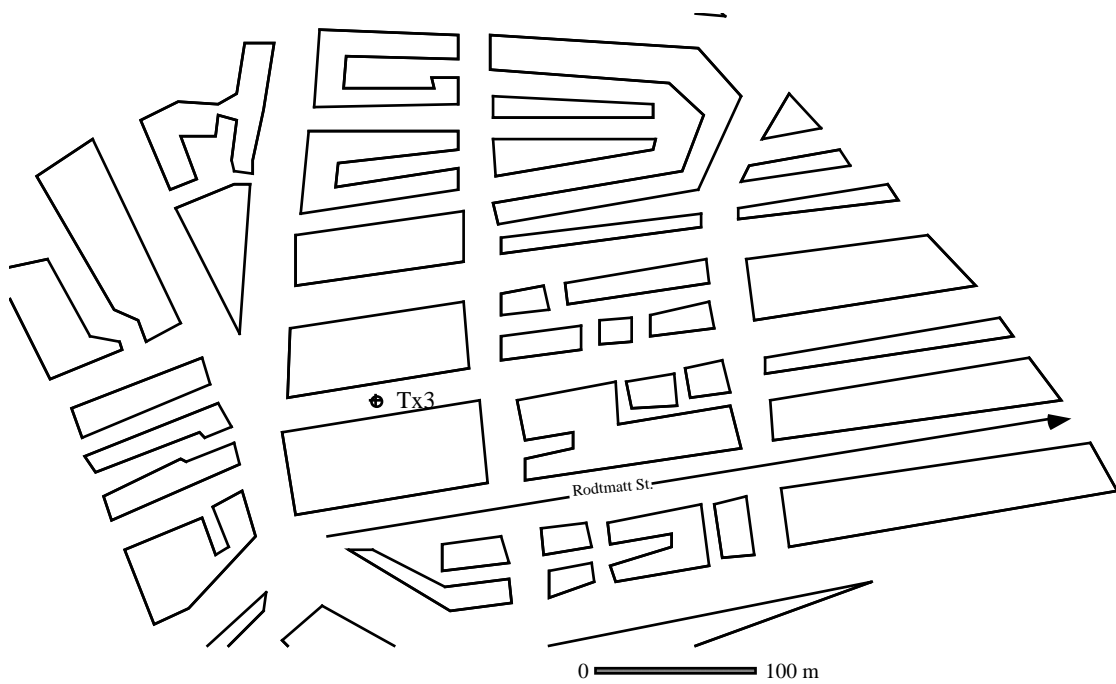


Fig. 2. City map. The cross indicates the transmitter location. The arrowed line represents the observation route driven in the direction indicated by the arrow.

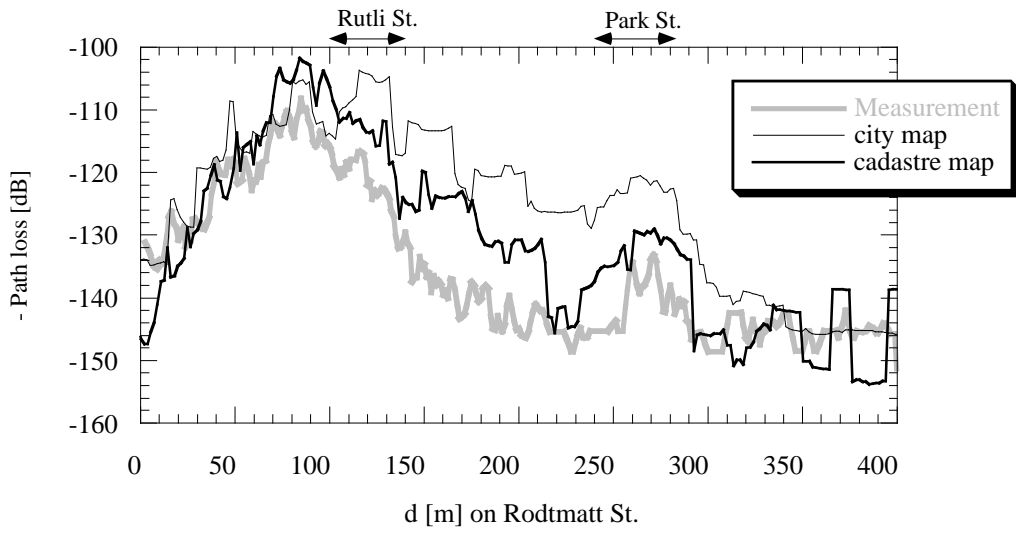


Fig. 3. Comparison on Rodtmatt St. between measurements and predictions using the city map and cadastre map as the vector database.

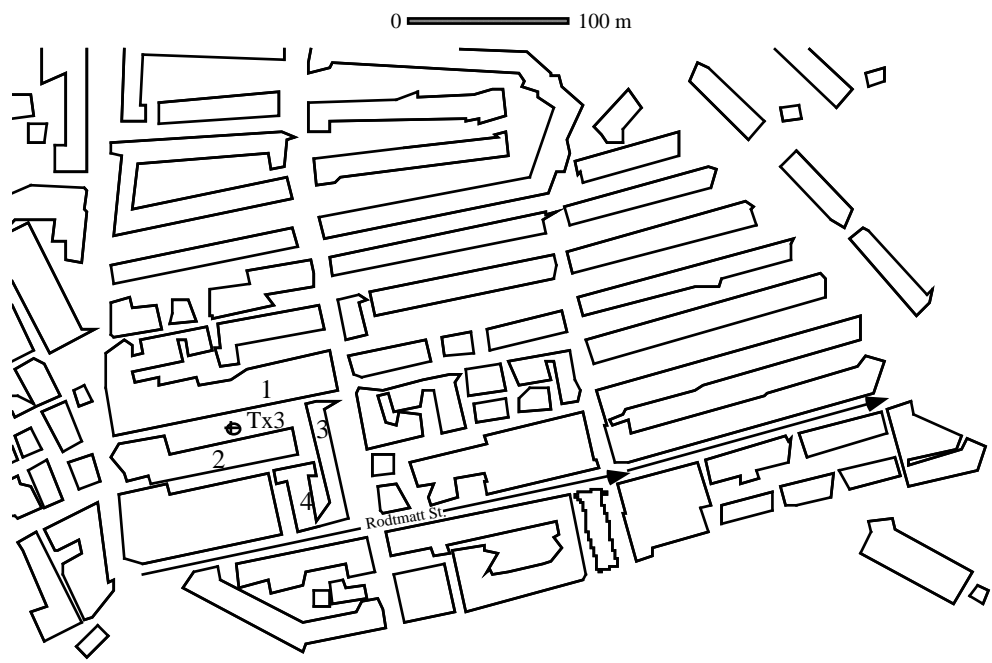


Fig. 4. 1:25000 map. The cross indicates the transmitter location. The arrowed line represents the observation route driven in the direction indicated by the arrow.

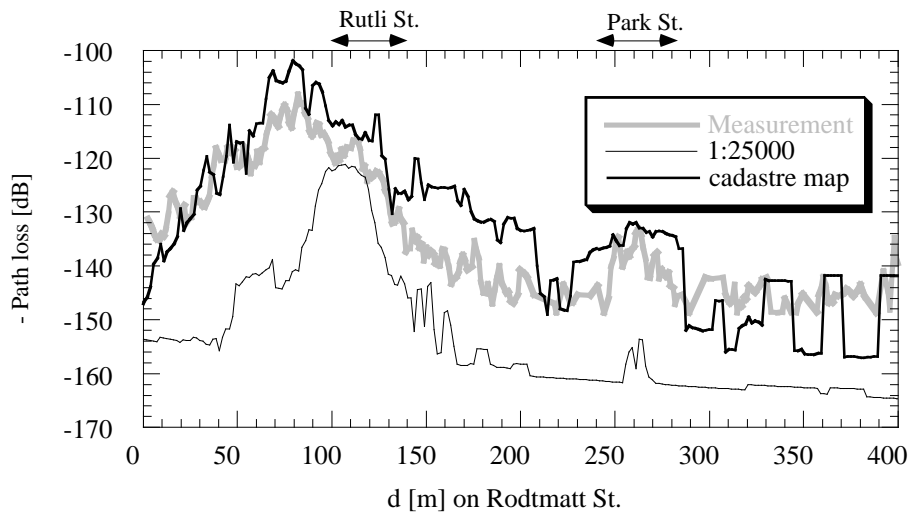


Fig. 5. Comparison on Rodtmatt St. between measurements and predictions using the 1:25000 map and the cadastre map as the vector database.

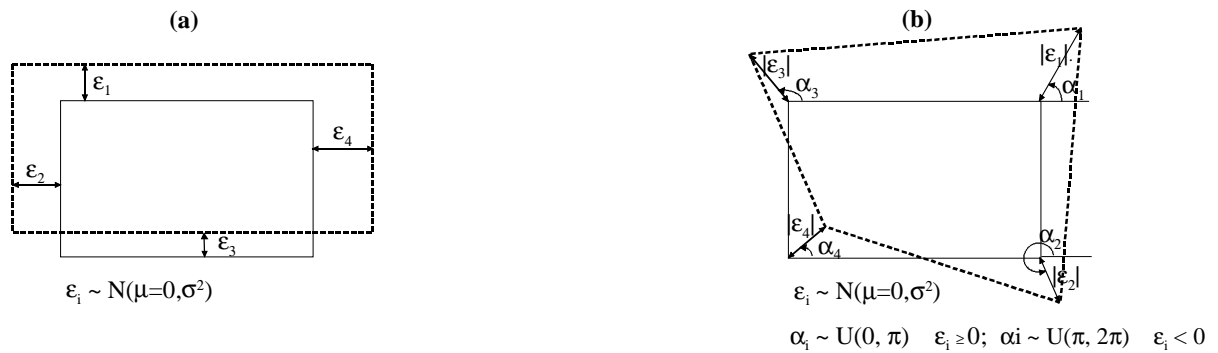


Fig. 6. Two types of errors in a map. (a) Error in Building size; the orientation of the building walls is kept constant, (b) Error in vertex position. The term  $N(\mu, \sigma^2)$  denotes a normal distribution with  $\mu$  and  $\sigma$  as mean and standard deviation. The term  $U(a1, a2)$  denotes a uniform distribution with  $a1$  and  $a2$  as lower and upper limits of the variation.

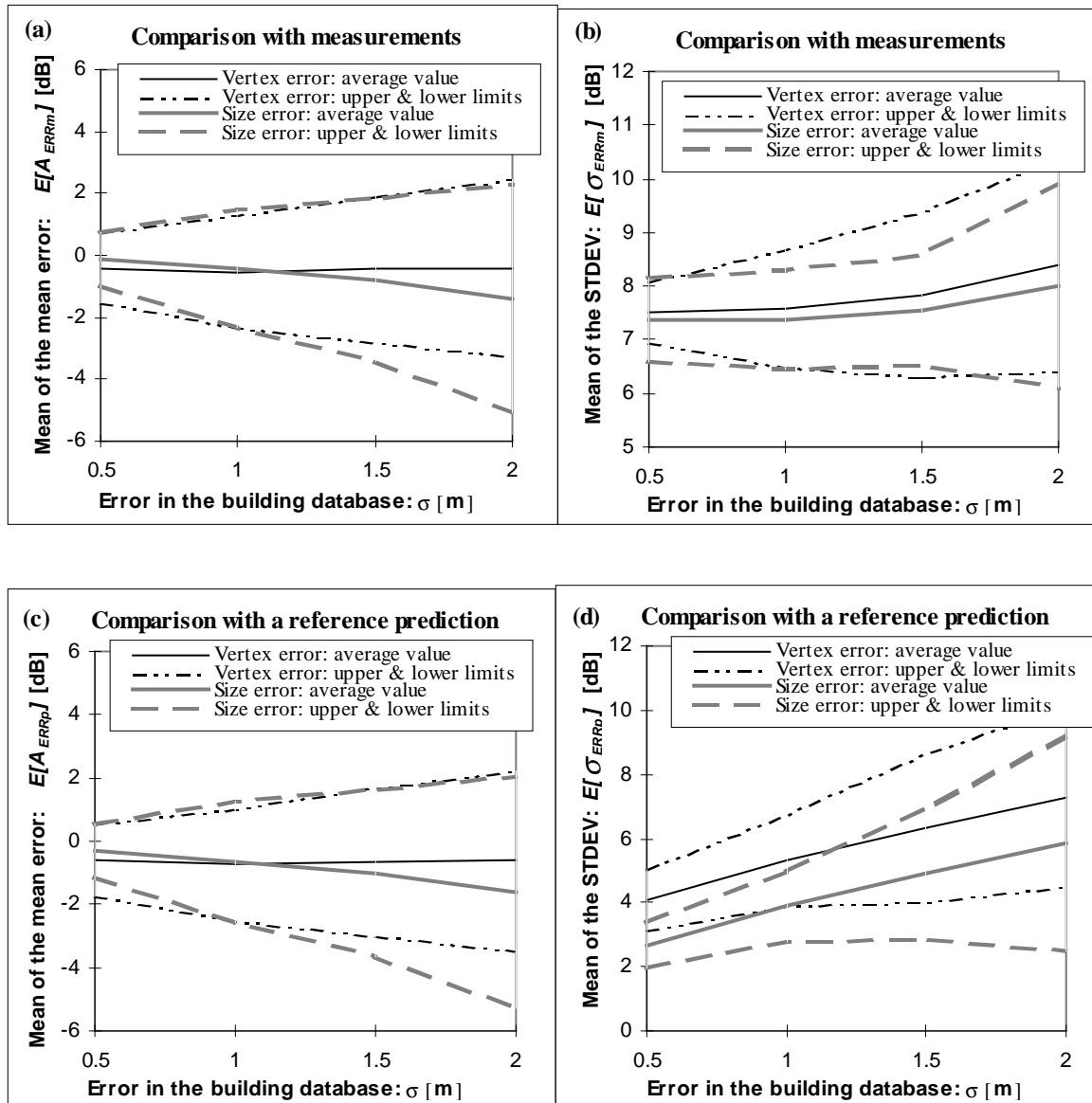


Fig. 7. (a) & (b) The average error and the standard deviation of the difference between predictions using the map with random errors and measurements. (c) & (d) The average error and the standard deviation of the difference between predictions using the maps with random errors and predictions using the original cadastre map.

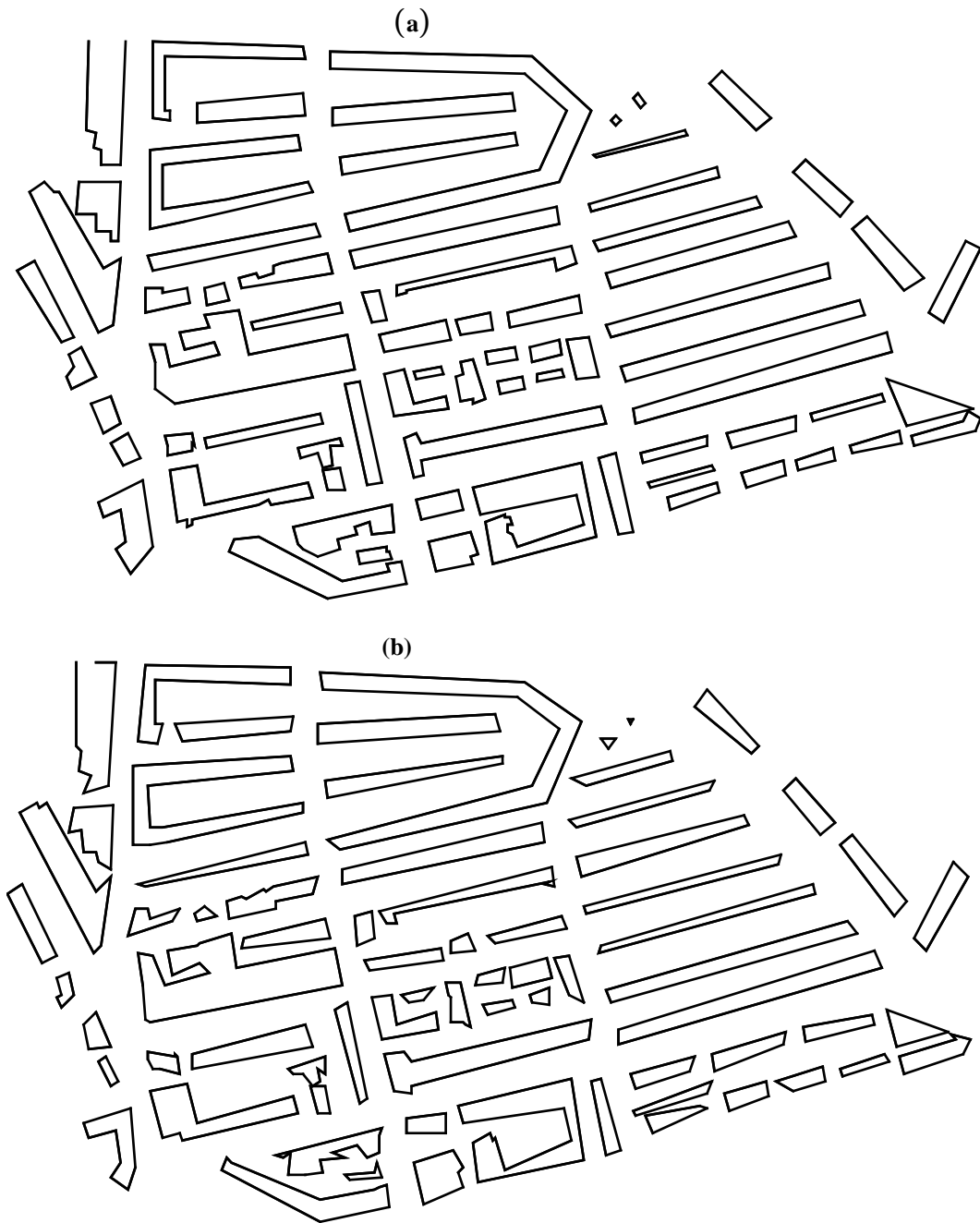


Fig. 8. Two realizations of an artificially erroneous map with: (a) random error in building size ( $\sigma = 2$  m) and (b) random error in the vertex position ( $\sigma = 2$  m), The original map without deformation is shown in Fig. 1.

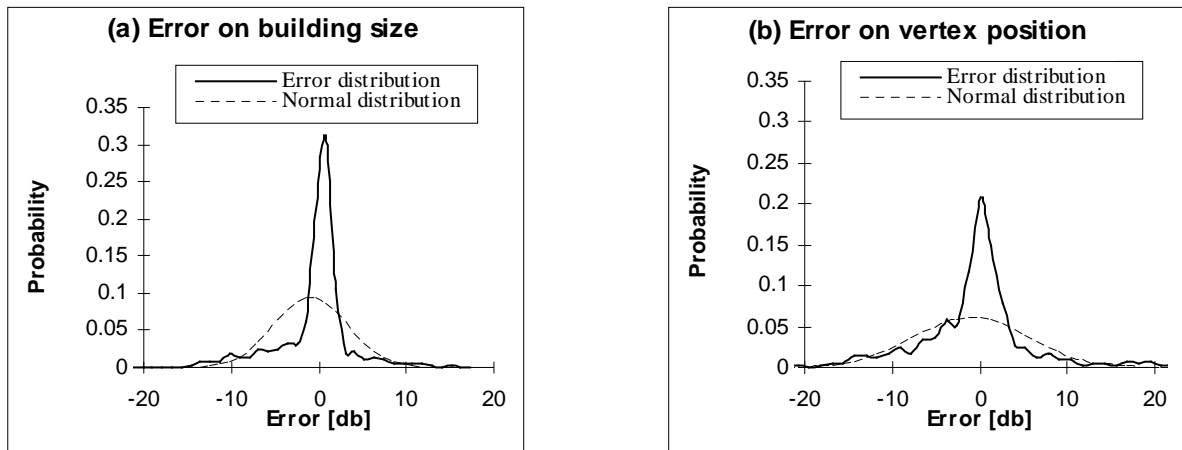


Fig. 9. Distribution function of the errors between the reference prediction using the cadastre map and the predictions using two realizations of an erroneous map due to: (a) error in Building size ( $\sigma_{\epsilon} = 1$  m), (b) error in vertex position ( $\sigma_{\epsilon} = 1$  m).

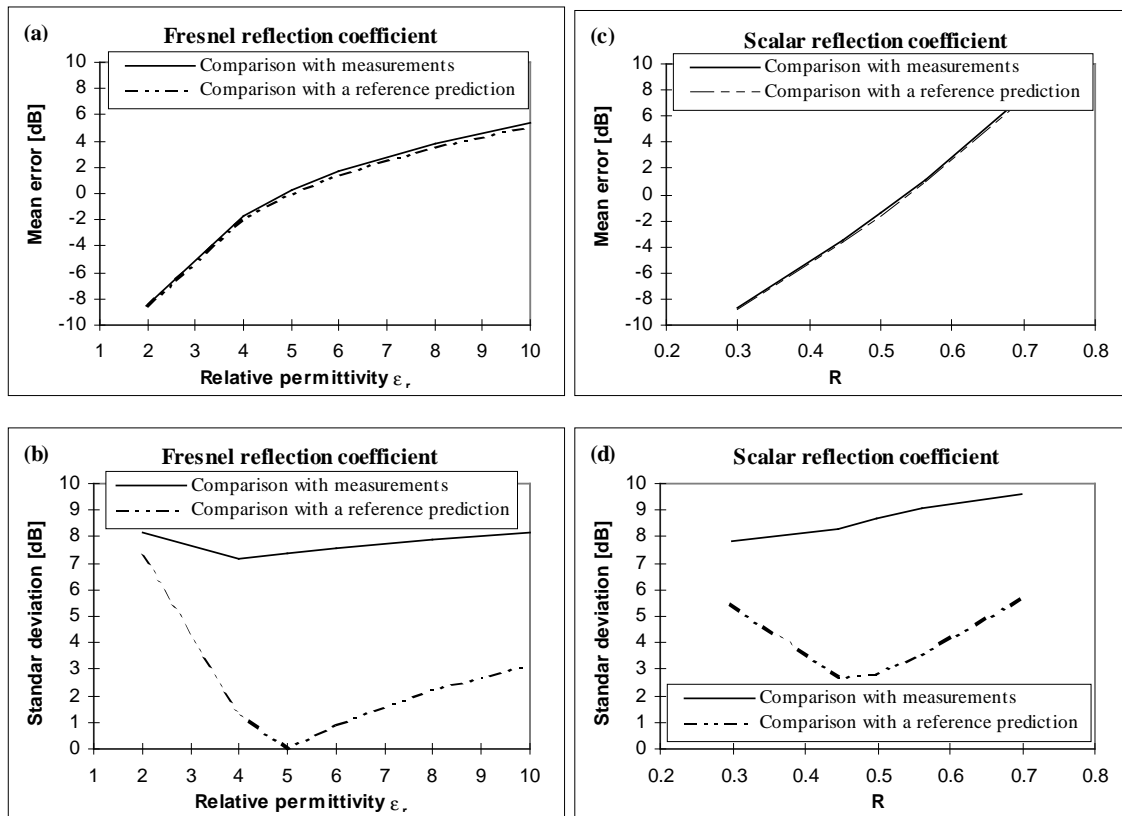


Fig. 10. (a & b) the mean error and standard deviation between predictions and measurements or the reference prediction when the permittivity varies. (c & d) the mean error and standard deviation between predictions and measurements or the reference prediction when the R varies.

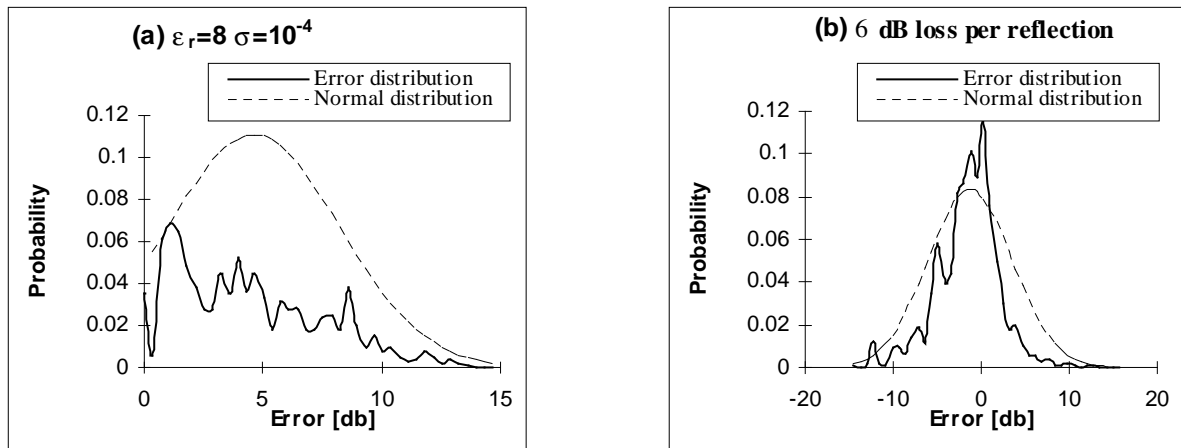


Fig. 11. Distribution function of the errors between the reference prediction ( $\epsilon_r = 5$ ,  $\sigma = 10^{-4}$ ) and the predictions using two sets of reflection coefficients: (a)  $\epsilon_r = 8$ ,  $\sigma = 0.10^{-4}$  [S/m] and (b) 6 dB loss/reflection.

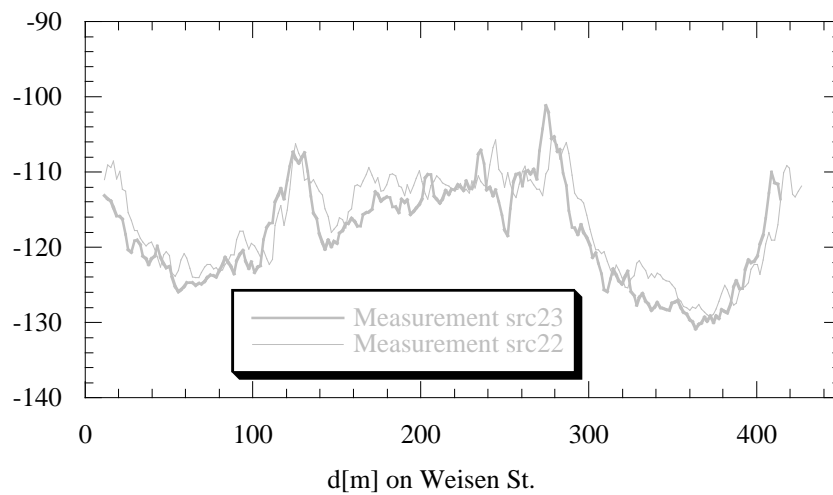


Fig. 12. Comparison on Wiesen St. between two measurements for two base station locations ( $Tx23$  and  $Tx22$  in Fig. 1).

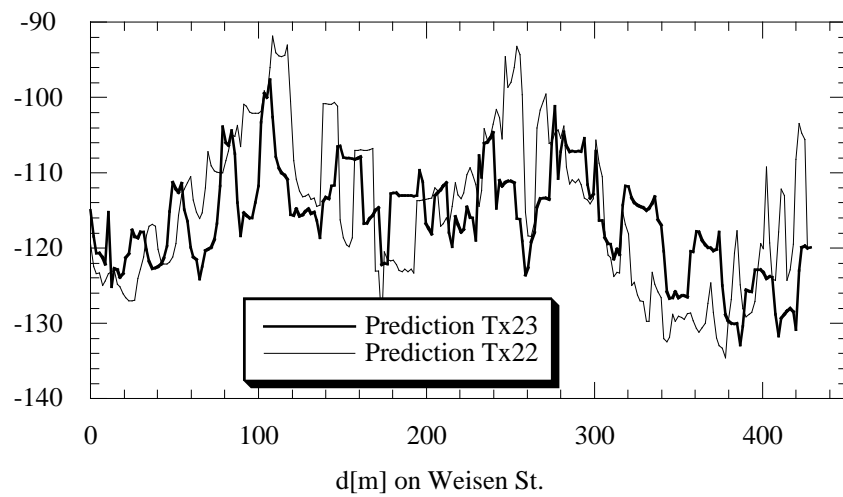


Fig. 13. Comparison on Wiesen St. between two predictions for base station locations ( $Tx23$  and  $Tx22$  in Fig. 1). The cadastre map is used as the vector database.